

Spherical-wave effects in photoelectron diffraction

M. Sagurton,* E. L. Bullock, R. Saiki, A. Kaduwela, C. R. Brundle,[†] and C. S. Fadley
Department of Chemistry, University of Hawaii, Honolulu, Hawaii 96822

J. J. Rehr

Department of Physics, University of Washington, Seattle, Washington 98195

(Received 27 August 1985)

The influence of spherical-wave (SW) effects on the analysis of photoelectron diffraction (PD) data is considered by comparing full SW single-scattering calculations with similar calculations based upon the plane-wave (PW) approximation and a new approximation for including SW effects (SW⁽¹⁾) due to Rehr, Albers, Natoli, and Stern, as well as with experimental data involving both scanned-energy and scanned-angle measurements. In general, SW effects are found to be much more important in forward scattering and to explain prior empirical adjustments of PW x-ray PD scattering amplitudes at higher energies of ≥ 500 eV. The more easily used SW⁽¹⁾ approximation is also seen to allow very well for SW effects. Not all PD data are expected to be equally sensitive to SW corrections. For example, scanned-energy data for S/Ni(001) emphasizing backscattering events are about equally well described by the PW and SW models, whereas higher-energy azimuthal-scan data for O/Ni(001) in which forward scattering is dominant require SW corrections to describe some, but not all, directions of emission quantitatively.

Core-level x-ray photoelectron diffraction (XPD) in which intensities are measured as a function of either emission angles¹⁻⁷ or photoelectron energy⁸ has by now become a very useful probe of surface structure. In analyzing such data, a simple single-scattering cluster (SSC) model in which each electron-atom scattering event at a scatterer j is treated via plane-wave (PW) scattering

factors $f_j(\theta_j)$ has been found in a number of prior studies to yield rather good agreement with a variety of PD measurements at ≥ 200 eV, including those involving both scanned-angle¹⁻⁷ and scanned-energy^{9,10} data. In the SSC model with PW scattering, the photoelectron intensity $I(\hat{\mathbf{k}})$ for s -level emission in the direction $\hat{\mathbf{k}}$ and with radiation polarization $\hat{\mathbf{e}}$ is given by^{2,4}

$$I(\hat{\mathbf{k}}) \propto \left| \hat{\mathbf{e}} \cdot \hat{\mathbf{k}} \exp(-L/2\Lambda_e) + \sum_j \frac{\hat{\mathbf{e}} \cdot \hat{\mathbf{r}}_j}{r_j} |f_j(\theta_j)| W_j \exp(-L_j/2\Lambda_e) \exp\{i[kr_j(1 - \cos\theta_j) + \Psi_j(\theta_j)]\} \right|^2, \quad (1)$$

where L and L_j are path lengths for inelastic scattering, Λ_e is the inelastic attenuation length, r_j is the distance from emitter to scatterer j , and $\hat{\mathbf{r}}_j$ is the direction vector to j , W_j is the Debye-Waller factor for scatterer j , k is the electron wave vector, and $\Psi_j(\theta_j)$ is the phase shift associated with $f_j(\theta_j)$. However, the possible importance of spherical-wave (SW) scattering corrections in correctly predicting such XPD phenomena has long been recognized, and such corrections have been discussed in a few prior studies based on approximate treatments or limited to specific test cases.^{1,4,8,10-12} It is thus important in judging all forms of photoelectron diffraction as surface structure probes, to determine quantitatively in a more comprehensive way how strong such SW effects are, and to ask further how they can be conveniently incorporated into the SSC model to avoid calculations of a very cumbersome nature.

We have thus carried out a detailed comparison of the PW and SW approximations for the illustrative test case of a single Ni scatterer at a variable distance r away from a source of photoelectrons emitted at different energies from an s core level. Also, we have compared PW and

SW results for much larger clusters of 120–300 atoms appropriate to the simulation of both scanned-angle and scanned-energy experimental data. The SW model utilized is similar to that discussed previously for extended x-ray absorption fine structure,¹³ and involves no approximations other than that of single scattering.¹⁴ The effects of inelastic scattering and atomic vibration are included in the same phenomenological way as in prior PW calculations.^{2,4,9,10} In addition, an approximation for including SW corrections suggested recently by Rehr, Albers, and Natoli¹⁵ has been incorporated in some of our calculations. This will be denoted SW⁽¹⁾ and involves expanding the spherical Hankel functions $h_l^+(kr)$ appearing in the SW theory in a power series valid for large kr and keeping only the first terms in both amplitude and phase that go beyond the limiting form for large kr of (Ref. 12)

$$h_l^+(kr) \sim \exp[i(kr - l\pi/2)]/kr.$$

The correction factor to this limiting form thus becomes¹⁵

$$C_l(kr) \equiv \left[1 + \frac{l(l+1)}{2(kr)^2} \right]^{1/2} \exp[i l(l+1)/2kr].$$

The net limiting result is a calculation procedure in which an effective scattering factor $f_{\text{eff},j}(r, \theta_j)$ which depends on r takes the place of the usual PW $f_j(\theta_j)$. However, $f_{\text{eff},j}(r, \theta_j)$ is very easily calculable, so that the net increase in time for an SSC-SW⁽¹⁾ computation as compared to an SSC-PW computation is less than a factor of two. By contrast, a full SSC-SW computation requires about 20 times the time of the analogous SSC-PW computation.

As a first comparison of these three methods, Fig. 1 shows the single-scatterer polar photoelectron diffraction patterns for a Ni atom at the bulk Ni nearest-neighbor distance of 2.49 Å away from an *s*-level emitter over a broad range of energies from 50 to 950 eV. The photoelectron wave is thus *p* type. The radiation polarization \hat{e} is held parallel to the electron emission direction \hat{k} . Here we plot the normalized intensity modulation

$$\chi = [I(\theta_{\text{Ni}}) - I_0(\theta_{\text{Ni}})] / I_0(\theta_{\text{Ni}}),$$

where θ_{Ni} is the scattering angle, I is the intensity with the scatterer present, and I_0 is the reference intensity in the absence of the scatterer. The fine-scale oscillations in χ , which decrease in period at higher energies, are due to interference between direct and scattered waves, with phase differences caused principally by the path-length difference of $r(1 - \cos\theta_{\text{Ni}})$. Such oscillations are well known in such two-atom photoelectron diffraction geometries.^{1,4,7(b),7(c)}

Figure 1 directly permits us to make the following conclusions: SW effects (as judged by the difference between the SW and PW curves) are important in *both* forward-scattering and backscattering directions for energies ≤ 100 eV, but for energies > 200 eV they are significant only for scattering angles $\leq 40^\circ - 50^\circ$. The forward peaking in the diffraction intensity that has been emphasized in a number of prior discussions of XPD at ≥ 500 eV (Refs. 1–4 and 7) is also evident in both the PW and SW curves. However, the SW curves always exhibit a weaker forward peaking, a difference which is enhanced as energy is increased. Thus, for experiments emphasizing backscattering at energies ≥ 200 eV, SW effects are expected to be much less important, and this is qualitatively consistent with prior PW analyses of synchrotron radiation data involving strong backscattering at > 200 eV of both the scanned-angle⁶ and scanned-energy^{9,10} types. [We will make a detailed comparison of PW and SW results for scanned-energy data from $c(2 \times 2)\text{S}/\text{Ni}(001)$ below.] As a final point concerning Fig. 1, we note that the SW⁽¹⁾ approximation is in excellent agreement with all of the major χ features of the full SW curves, with the only noticeable, but nonetheless small, discrepancies being for energies ≤ 100 eV and weaker features at intermediate scattering angles of $\sim 40^\circ - 140^\circ$. The agreement between SW⁽¹⁾ and SW is essentially perfect in the more important forward and backward directions for all energies.

The greater importance of SW effects in forward scattering is also easily explained for higher energies via a qualitative classical argument. Forward scattering involves small trajectory deflections and thus is expected to be more sensitive to the weaker outer regions of the scattering potential (that is, for larger radii from the scattering center); the converse should thus be true for

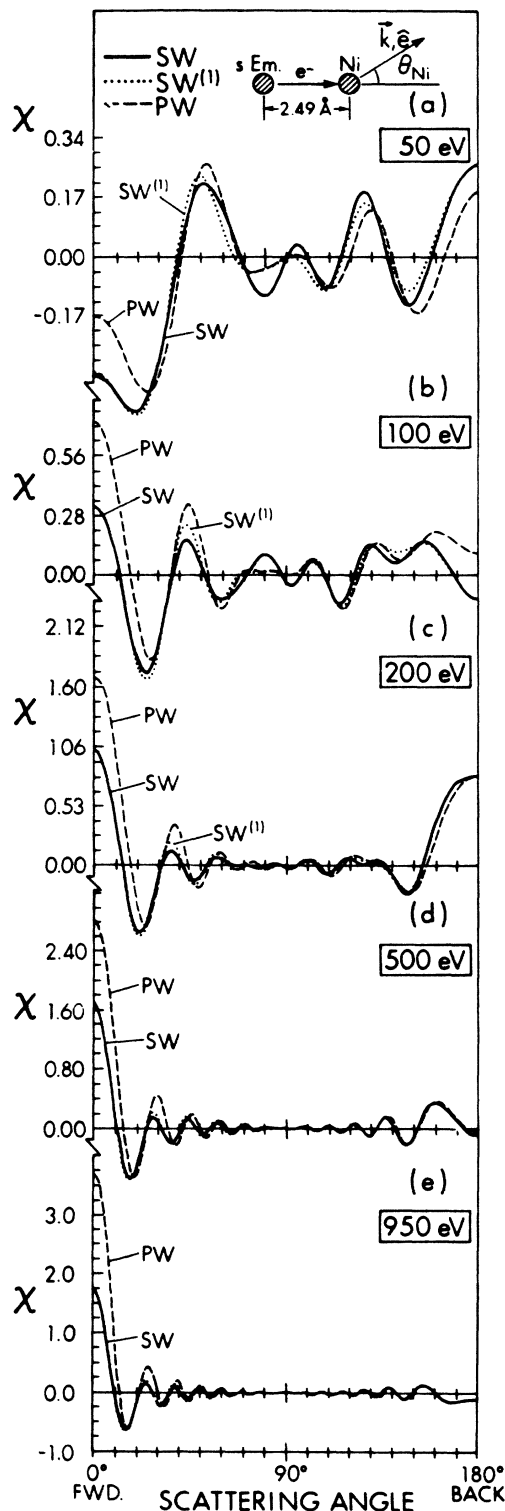


FIG. 1. Theoretical χ curves for emission from an *s* level as a function of the scattering angle θ_{Ni} for a single Ni scatterer at a distance of 2.49 Å from the emitter (Em). Polarization is parallel to the emission direction. The three approximations PW, SW, and SW⁽¹⁾ are shown for energies of 50–950 eV.

backscattering with very large deflections of $\sim 180^\circ$. Thus, in backscattering the effective potential occupies a smaller volume, and wave curvature over this volume is more easily neglected. This qualitative conclusion is further confirmed by the sensitivity of quantum-mechanically calculated PW $f(\theta)$ values to the effective radius of the scattering potential. That is, if the free-atom $f(\theta)$ values of Fink and co-workers¹⁶ are compared with analogous $f(\theta)$ values calculated for muffin-tin potentials of smaller radii, it is found that the two calculations agree extremely well as to both the amplitude and phase of $f(\theta)$ for $\theta > 20^\circ$, but for $\theta < 20^\circ$, the atomic $|f(\theta)|$ values are systematically larger, with, for example, the atomic $|f(0)| \approx 1.3$ – 2.0 times the muffin-tin $|f(0)|$.^{2,17} This result also suggests that the calculation of forward-scattering amplitudes will be sensitive to the muffin-tin radius chosen, and direct calculations confirm this: a larger radius yields a larger $|f(0)|$.

A further consequence of this enhanced sensitivity of forward-scattering amplitudes to the outer regions of the potential is seen in more recently discussed spin-polarized photoelectron diffraction (SPPD) measurements, for which scattering from atoms or ions with a net spin is involved.¹⁸ Here, it is the charge density associated with unpaired valence electrons [e.g., in $\text{Mn}^{2+} 3d^5(\uparrow\uparrow\uparrow\uparrow)6S$] that is responsible for the spin-dependent exchange interaction producing SPPD. Spin-up photoelectrons will thus be scattered slightly differently from spin-down electrons by Mn^{2+} due to exchange with the $3d$ electrons. Because the $3d$ valence charge density is primarily located at larger radii corresponding to the outer extremities of the scattering potential of a given Mn^{2+} ion, we would expect greater SPPD effects in forward scattering, in complete agreement with direct calculations of spin-dependent scattering factors for Mn^{2+} .¹⁸ In these calculations, the forward-scattering spin asymmetries are found to be approximately two times greater than those of backscattering.

It is now also of interest to ask how rapidly the PW limit is reached as the distance between emitter and scatterer is increased, again for the single-scatterer case of Fig. 1. In Fig. 2 we thus show χ curves for three distances of one, two, and three times the nearest-neighbor distance of 2.49 Å and for two energies of 200 eV [Fig. 2(a)] and 500 eV [Fig. 2(b)]. For both energies, it is clear that SW effects decrease as r increases, and that the PW limit is reached first for scattering angles $> 40^\circ$ – 50° . However, in the forward direction the PW limit is not fully reached for either energy by the last case shown of $r = 7.5$ Å. Similar results are also found for energies up to 1420 eV that are typical of XPD measurements with standard x-ray sources. The $\text{SW}^{(1)}$ curves in Fig. 2 are again in excellent agreement with the SW curves, hardly differing enough to be shown as distinct curves for the two larger distances. Analogous comparisons for other polarization orientations with respect to \mathbf{k} also show good agreement between $\text{SW}^{(1)}$ and SW curves. Thus, this approximation¹⁵ seems very encouraging as a computationally convenient method for incorporating SW effects into photoelectron diffraction theory.

We now focus specifically on the forward-scattering re-

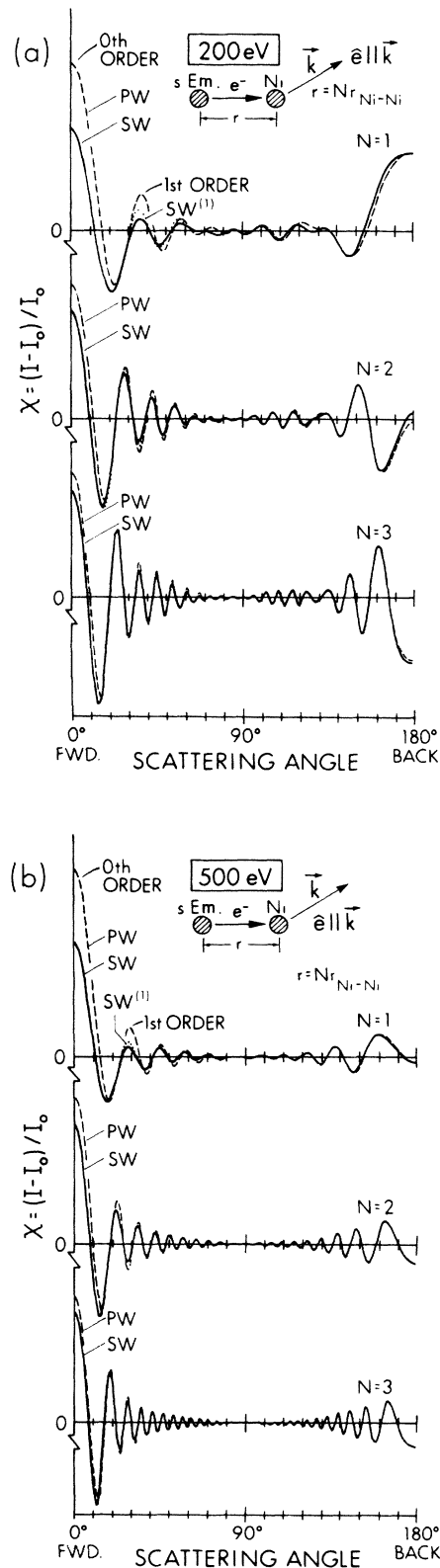


FIG. 2. Theoretical χ curves for the same geometry as Fig. 1, but with variable scatterer distances of 2.49, 4.98, and 7.47 Å and two energies of (a) 200 eV and (b) 500 eV. "0-th order" here implies forward scattering ($\theta_{\text{Ni}}=0$) in which the only phase shift in Eq. (1) is due to $\Psi_{\text{Ni}}(0)$, and "1st order" indicates an overall phase shift of $kr(1 - \cos\theta_{\text{Ni}}) + \Psi_{\text{Ni}}(\theta_{\text{Ni}}) = 2\pi$ (Ref. 1).

gion that is strongest in the χ curves for all energies and comes to dominate them fully for energies ≥ 500 eV. In Fig. 3 we plot the ratio $\chi(\text{SW})/\chi(\text{PW})$ evaluated at $\theta_{\text{Ni}}=0^\circ$ as a function of the scatterer distance, again in units of 2.49 Å. Curves are shown for a broad range of energies from 100 to 1420 eV, and all show a rather similar shape, with $\chi(\text{SW})/\chi(\text{PW})$ in the range of 0.24–0.47 for the smallest distance considered of 1.75 Å and with a smooth convergence to a value of 1.00 as distance is increased. (1.75 Å is chosen to represent a minimum possible bond length from Ni to an emitter that could possess a core level.) However, we note that this convergence to 1.00 is reasonably slow, with values of ~ 0.88 – 0.93 for 12.5 Å and of ~ 0.93 – 0.97 for 20.0 Å. Thus, even at the outer reaches of a cluster of radius 20 Å centered around an emitter, SW effects are still present in forward scattering; however, it is also clear that these effects are, as expected, strongest in the first few spheres of neighbors. We also note that $\chi(\text{SW})/\chi(\text{PW})$ values calculated in the SW⁽¹⁾ approximation are found to agree excellently with the results of Fig. 3, in all cases to within the linewidths of the curves.

The results in Fig. 3 also permit us to explain the empirical adjustment of PW scattering-factor amplitudes $|f(\theta)|$ by factors of ~ 0.4 – 0.5 , which has been found in several prior XPD studies to improve somewhat the agreement with experiments at > 500 eV.^{2,4,7,19} That is, since forward scattering from nearest-neighbor and next-nearest-neighbor atoms is expected to dominate in producing the major features in such higher-energy photoelectron diffraction curves,^{2,4,7} a zeroth-order method of correcting the PW model would be simply to multiply $|f(\theta)|$ by the appropriate forward-scattering ratio of $\chi(\text{SW})/\chi(\text{PW})$. Indeed the values of $\chi(\text{SW})/\chi(\text{PW})$ found here for Ni nearest-neighbor distances are very close to the 0.4–0.5 factors found empirically. Since nearest neighbors will also be the strongest scatterers in a given problem, we thus ascribe the principle source of this prior empirical adjustment to SW effects. The fact that Figs. 1 and 2 qualitatively support such a straightforward

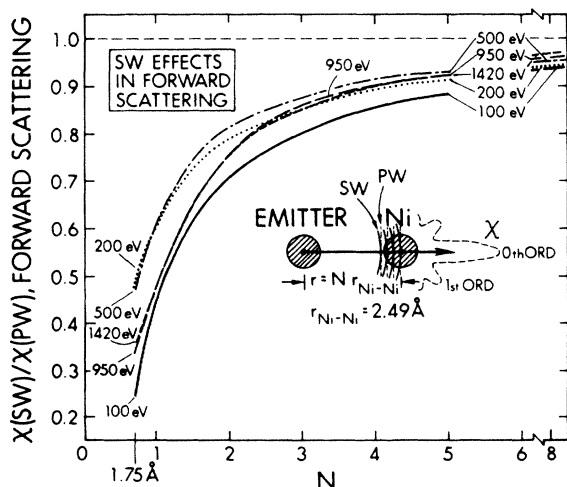


FIG. 3. Theoretical forward scattering ($\theta_{\text{Ni}}=0^\circ$) ratios of $\chi(\text{SW})/\chi(\text{PW})$ are shown as a function of scatterer distance from 1.75 to 19.92 Å and for energies of 100–1420 eV.

forward-scattering amplitude reduction due to SW effects also explains why the simple PW model has proven successful in interpreting higher-energy XPD data. The PW model may predict effects of a higher magnitude than would be the case with a SW approach, but most features are correctly predicted as to position and relative intensity.^{1–4,7}

A closer inspection of Figs. 1 and 2 indicates, however, that not only an *amplitude* correction of PW results is needed, but also a *phase* correction, as the maxima, minima, and zeroes in the SW and PW χ curves occur at slightly different θ_{Ni} values for the curves at smaller r corresponding to near-neighbor positions. This is confirmed by an analysis of the f_{eff} values obtained from the SW⁽¹⁾ approximation: For example, at $r=2.49$ Å and 500 eV, $|f_{\text{eff}}(\theta=0)|=2.91$ Å and is actually 11% larger than the PW $|f(\theta=0)|=2.62$ Å, but the phase of $f_{\text{eff}}(0)$ is 83° compared to only 44° for $f(0)$. Thus, the simple amplitude correction applied in previous XPD analyses is not expected to be a fully accurate way of including SW effects in forward scattering, even though it clearly has led to improved agreement with experiment in several cases.^{2,4,7,19}

We now consider two examples of more complex multiscatterer SSC calculations that can be directly compared to corresponding experimental data. In Fig. 4, scanned-energy sulfur 1s data obtained by Barton *et al.*⁸ for $c(2 \times 2)\text{S}/\text{Ni}(001)$ in the experimental geometry shown in the inset are compared to PW and SW calculations for a cluster of 120 S and Ni atoms. The calculations make use of a reasonably accurate correlated-vibration model discussed elsewhere.¹⁰ Both $\chi(E)$ curves and Fourier transforms (FT's) of $\chi(E)$ curves are shown. The $\chi(E)$ curves in Fig. 4(a) are, in general, in very good to excellent agreement. The experimental features *a*, *c*, *d*, *e*, *f*, *g*, *h*, *i*, and *j* are all very well predicted by the PW or SW curves, with the two theory curves also showing essentially identical features. The only minor discrepancies between experiment and theory are the nonresolution of features *b* and *c*, the relatively small peak shifts of ~ 11 eV for peak *a* and ~ 14 eV for peak *f*, and a somewhat low intensity in theory for peak *i*. There are also only very minor differences between the PW and SW χ curves: features *d* and *e* are stronger in the PW curve and there is a stronger upward slope in the PW curve for energies ≥ 225 eV. This close similarity of the PW and SW results is also seen in the FT's of Fig. 4(c), which show essentially the same peaks, but with some small peak shifts and shape changes, as well as significantly higher amplitudes for the PW peaks at path-length differences < 3.0 Å. Overall, these PW-SW comparisons thus verify that SW corrections are of lesser importance for this particular experiment, which overall tends to emphasize near-neighbor backscattering.^{8,10} Figure 4(b) finally compares an experimental FT obtained with an autoregressive (AR) range extension procedure⁸ to a SW FT taken over a broader energy interval of 40–600 eV so as to simulate the AR FT procedure. In general, there is also very good agreement here as to the position and relative intensities of the four major experimental peaks at 3.4, 4.4, 7.2, and 9.2 Å, thus further confirming the general utility of SSC calculations in the

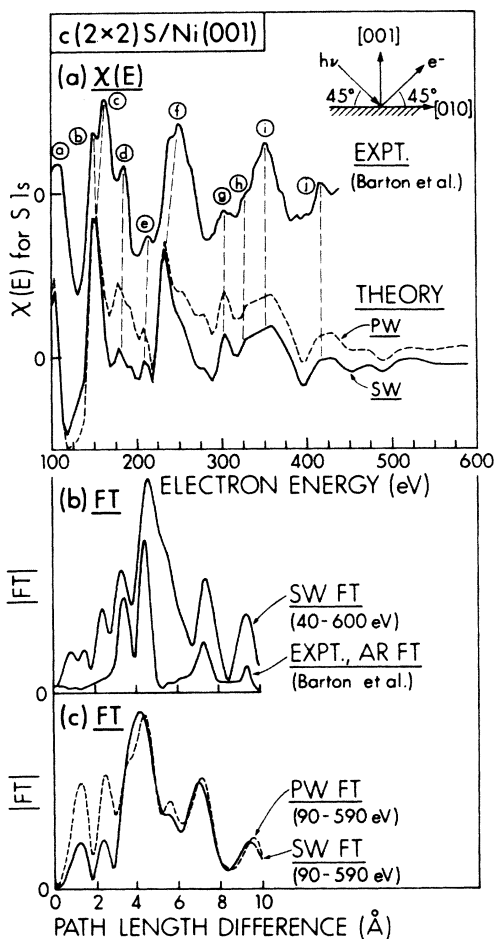


FIG. 4. Experimental and theoretical energy scans of the S 1s intensity from $c(2 \times 2)S/Ni(001)$, with the experimental geometry of Ref. 8 shown in the inset. In (a) the experimental S1s $\chi(E)$ curve is compared to analogous PW and SW theory curves. In (b) an experimental Fourier transform (FT) based on autoregressive (AR) methods (Ref. 8) is compared to a SW FT over the extended range of 40–600 eV. In (c) PW and SW FT's over the range 90–590 eV are compared.

analysis of such data.

As a final comparison of PW and SW results to experimental data, we show in Fig. 5 azimuthal scans of the oxygen 1s intensity as excited by Al $K\alpha$ radiation from a $c(2 \times 2)$ oxygen overlayer on Ni(001). The electron kinetic energy is ~ 950 eV, and the polar angle of emission with respect to the surface is $\theta = 7.0^\circ$ [Fig. 5(a)] or 13.3° [Fig. 5(b)]. From prior studies involving several structural probes, it is thought that oxygen bonds in a fourfold-hollow site at ~ 0.8 – 0.9 Å above the Ni surface,²⁰ although a slightly offset pseudobridge structure also has been suggested more recently by Demuth *et al.*²¹ based on a low-energy electron diffraction analysis. Simple fourfold PW and SW curves are shown for the distances of 0.90 and 0.95 Å above the surface, which were obtained by optimally matching theory and experiment. Analogous SW calculations for the offset geometry of Ref. 21 are also shown. All calculations were for clusters of ~ 300 atoms with correlated vibrations.¹⁰ It is quite clear that the simple fourfold SW curves describe the experimental

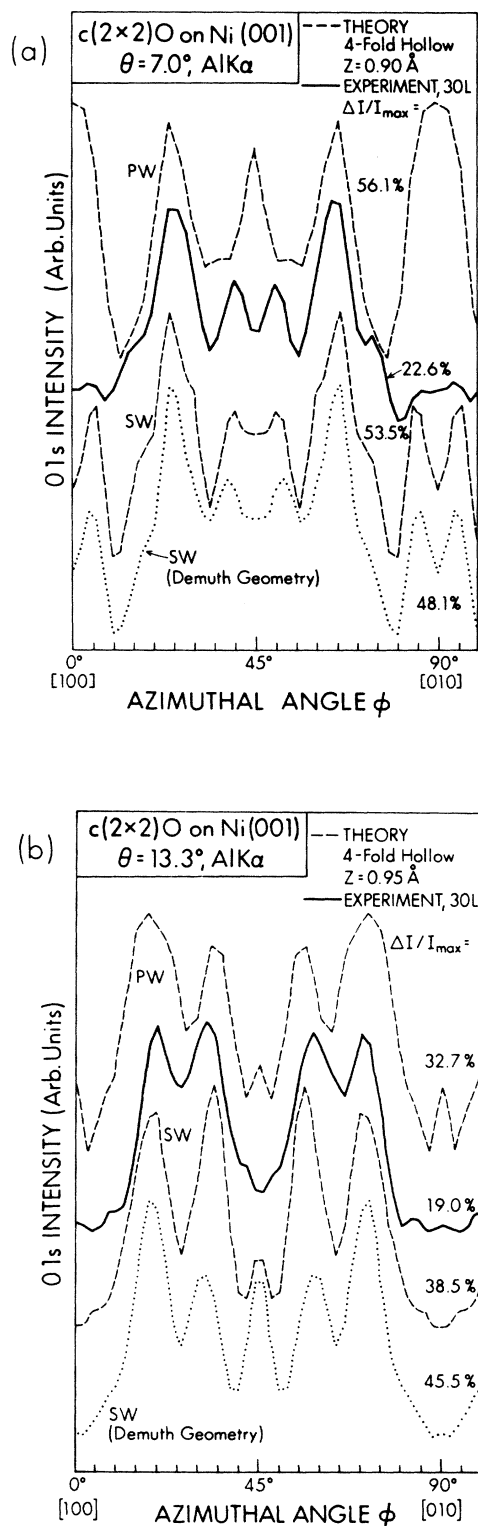


FIG. 5. Experimental and theoretical azimuthal scans of the O 1s intensity from $c(2 \times 2)O/Ni(001)$ at angles θ of emission with respect to the surface of (a) 7.0° and (b) 13.3° . The experimental data are for an exposure of 30 langmuirs (30 L) ($1 \text{ L} = 10^{-6} \text{ Torr sec}$). PW and SW theory curves are shown for the simple fourfold geometry at vertical distances of (a) 0.90 Å and (b) 0.95 Å. Also shown are SW curves for the pseudobridge structure of Ref. 21 proposed by Demuth *et al.*

data excellently.

In Fig. 5(a) all peaks and shoulders for $10^\circ < \phi < 80^\circ$ are very well described as to positions and relative intensities; only the doublet centered at $\phi = 0^\circ$ or 90° is too strong in theory, although there is in fact a suggestion of it in the experimental curve. The PW results in Fig. 5(a) are by contrast in very poor agreement, with only the positions of the two symmetry-related peaks at $\phi = 25^\circ$ and 65° being predicted and all other features severely out of agreement. Note, in particular, the dramatic decrease of the intensity along the [100]-type azimuths in going from the PW curve to the SW curve. This is due to a reduction in the strong forward scattering by nearest-neighbor oxygen atoms in the $c(2 \times 2)$ overlayer, which lie directly along these azimuths at a distance of 3.52 Å. Similar anomalously strong PW forward-scattering peaks have previously been seen for low- θ nearest-neighbor scattering in $c(2 \times 2)$ S and $c(2 \times 2)$ Se on Ni(001),^{3,4} but their suggested explanation in terms of spherical-wave effects is now substantiated. The SW curve for the pseudobridge geometry²¹ in Fig. 5(a) is very similar to the simple fourfold curve, but is not in quite as good agreement with experiment, exhibiting a reduction of the shoulders at $\phi = 15^\circ$ and 75° and a broadening of the separation of the doublet at $\phi = 45^\circ$ that are not seen in experiment.

Figure 5(b) shows a similar comparison of experiment and theory, but with slightly different conclusions. Again, the simple fourfold SW curve best agrees with experiment, but for this higher- θ data at 13.3° , the PW and SW curves are not so different. Both curves show the same general four-peak structure, with minor differences only in the shape and width of the peaks at $\phi \approx 20^\circ, 70^\circ$, and in the presence of small peaks at $\phi = 0^\circ, 90^\circ$ only in the PW curve. The SW curve does agree slightly better with experiment however. The pseudobridge geometry is much less favored as the structure of $c(2 \times 2)$ O/Ni(001) in Fig. 5(b), with its SW curve showing a strong peak at $\phi = 45^\circ$ that is missing in experiment, as well as incorrect relative intensities among the other four peaks. Similar compar-

isons of azimuthal curves for other polar angles of emission $\theta = 10.0^\circ$ and 16.0° yield the same general conclusions,²² with results at the highest two (13.3° and 16.0°) showing overall the least difference between PW and SW results. Thus, for $\theta \gtrsim 13^\circ$, PW calculations could probably be used to derive accurate conclusions concerning the $c(2 \times 2)$ structure. Overall, the simple fourfold hollow at 0.88 ± 0.10 Å is found for the structure, in agreement with prior work,²⁰ but not Ref. 21. A more detailed account of these O/Ni results is in preparation.²²

In conclusion, SW effects are expected to be important in both forward and backscattering for energies < 100 eV, but only in forward scattering for energies > 200 eV. (These breakpoints in energy may change slightly with the atomic number of the scatterer, or with changes in the effective radius of the potential, for example, through a muffin-tin choice.) The SW⁽¹⁾ approximation of Ref. 15 is also found to rather accurately include SW effects in a manner that is very convenient to calculate. Prior empirical adjustments of forward-scattering PW amplitudes $|f_j(\theta_j)|$ at higher energies are explained in terms of SW effects, although additional phase corrections are also found to be important. PW and SW results are found to be rather close for scanned-energy data from $c(2 \times 2)$ Si/Ni(100) that emphasize backscattering. However, SW results are overall found to be in significantly better agreement with experiment for azimuthal data from the system $c(2 \times 2)$ O/Ni(001), especially for the lowest takeoff angles studied. Thus, the degree of need for inclusion of SW corrections in photoelectron diffraction depends strongly on the type of data to be analyzed. Although PW calculations already have described prior data in a reasonably accurate way, the most quantitative structural conclusions (particularly at higher energies where forward scattering is dominant) may require the inclusion of SW corrections.

This work was supported by National Science Foundation Grant No. CHE83-20200.

*Present address: National Synchrotron Light Source, Brookhaven National Laboratory, Upton, NY 11973.

†Permanent address: IBM Research, San Jose, CA 95193.

¹S. Kono, S. M. Goldberg, N. F. T. Hall, C. S. Fadley, and J. B. Pendry, *Phys. Rev. Lett.* **42**, 1545 (1979).

²S. Kono, S. M. Goldberg, N. F. T. Hall, and C. S. Fadley, *Phys. Rev. B* **22**, 6085 (1980).

³P. J. Orders, R. E. Connelly, N. F. T. Hall, and C. S. Fadley, *Phys. Rev. B* **24**, 6161 (1981).

⁴C. S. Fadley, in *Progress in Surface Sciences*, edited by S. Davison (Pergamon, New York, 1984), Vol. 16, p. 275, and references therein.

⁵B. Sinković, P. J. Orders, C. S. Fadley, R. Trehan, Z. Hussain, and J. Lecante, *Phys. Rev. B* **30**, 1833 (1984).

⁶P. J. Orders, B. Sinković, C. S. Fadley, R. Trehan, Z. Hussain, and J. Lecante, *Phys. Rev. B* **30**, 1838 (1984).

⁷(a) W. E. Egelhoff, *Phys. Rev. B* **30**, 1952 (1984); (b) H. C. Poon and S. Y. Tong, *ibid.* **30**, 6211 (1984); (c) E. L. Bullock and C. S. Fadley, *ibid.* **31**, 1212 (1985).

⁸J. J. Barton, C. C. Bahr, Z. Hussain, S. W. Robey, J. G. Tobin,

L. E. Klebanoff, and D. A. Shirley, *Phys. Rev. Lett.* **51**, 272 (1983); J. J. Barton, S. W. Robey, C. C. Bahr, and D. A. Shirley, in *The Structure of Surfaces* (Springer-Verlag, Berlin, 1985), p. 191, and references therein.

⁹P. J. Orders and C. S. Fadley, *Phys. Rev. B* **27**, 791 (1983); E. L. Bullock, C. S. Fadley and P. J. Orders, *ibid.* **28**, 4867 (1983).

¹⁰M. Sagurton, E. L. Bullock, and C. S. Fadley, *Phys. Rev. B* **30**, 7332 (1984).

¹¹H. Kasai, Y. Okumura, and A. Ohiji, *J. Phys. Soc. Jpn.* **52**, 14 (1983).

¹²J. J. Barton and D. A. Shirley, *Phys. Rev. B* **32**, 1892 (1985). Several methods of efficiently including SW effects in photoelectron diffraction calculations are discussed here, including one formally identical to SW⁽¹⁾.

¹³P. A. Lee and J. B. Pendry, *Phys. Rev. B* **11**, 2795 (1975).

¹⁴M. Sagurton, E. L. Bullock, and C. S. Fadley (unpublished); this work contains a detailed description of the SW method used here and its application to scanned-energy PD.

¹⁵J. J. Rehr and R. C. Albers, *Bull. Am. Phys. Soc.* **30**, 524

- (1985); J. J. Rehr, R. C. Albers, C. R. Natoli, and E. A. Stern (unpublished).
- ¹⁶M. Fink and A. C. Yates, *At. Data* **1**, 385 (1970); M. Fink and J. Ingram, *ibid.* **4**, 129 (1972).
- ¹⁷P. J. Orders and C. S. Fadley (unpublished).
- ¹⁸B. Sinković and C. S. Fadley, *Phys. Rev. B* **31**, 4665 (1985); B. Sinković, B. Hermsmeier, and C. S. Fadley, *Phys. Rev. Lett.* **55**, 1227 (1985).
- ¹⁹R. Trehan and C. S. Fadley (unpublished).
- ²⁰I. P. Batra and J. A. Barker, *Phys. Rev. B* **29**, 5286 (1984), and references therein.
- ²¹J. E. Demuth, N. J. DiNardo, and C. S. Gargill III, *Phys. Rev. Lett.* **50**, 1373 (1983).
- ²²R. Saiki, M. Sagurton, A. Kaduwela, C. R. Brundle, and C. S. Fadley (unpublished).